The Influence of South Pacific Convergence Zone Heating on the South Pacific Subtropical Anticyclone and Southern Hemisphere Storm Tracks

Abdullah A. Fahad*
Department of Atmospheric, Oceanic, and Earth Sciences, George Mason University, Fairfax, Virginia, USA.

Natalie J. Burls
Department of Atmospheric, Oceanic, and Earth Sciences, George Mason University, Fairfax, Virginia, USA.

Erik T. Swenson
Center for Ocean-Land-Atmosphere Studies, George Mason University, Fairfax, Virginia, USA.

David M. Straus
Department of Atmospheric, Oceanic, and Earth Sciences, George Mason University, Fairfax, Virginia, USA.

**Corresponding author address:* Abdullah A. Fahad, Department of Atmospheric, Oceanic, and Earth Sciences, George Mason University MSN 6C5, 4400 University Drive, Fairfax, VA 22030.
E-mail: afahad@gmu.edu

ABSTRACT

Subtropical anticyclones and midlatitude storm tracks are key components of the large-scale atmospheric circulation. Focusing on the southern hemisphere, the seasonality of the three dominant subtropical anticyclones, situated over the South Pacific, South Atlantic and South Indian Ocean basins, has a large influence on local weather and climate within South America, Southern Africa and Australasia, respectively. Generally speaking, sea level pressure within the southern hemisphere subtropics reaches its seasonal maximum during the winter season when the southern hemisphere Hadley Cell is at its strongest. One exception to this is the seasonal evolution of the South Pacific subtropical anticyclone. While winter maxima are seen in the South Atlantic and South Indian subtropical anticyclones, the South Pacific subtropical anticyclone reaches its seasonal maximum during local spring with elevated values extending into summer. In this study we investigate the hypothesis that strength of the austral summer South Pacific subtropical anticyclone is largely due to heating over the South Pacific Convergence Zone. Using reanalysis data, and AGCM added cooling and heating experiments to artificially change the strength of diabatic heating over the South Pacific Convergence Zone, our results show that increased heating triggers a Rossby wave train over the Southern Hemisphere mid-latitudes by increasing upper-level divergence. The propagating Rossby wave train creates a high-low sea level pressure pattern that projects onto the center of the South Pacific Subtropical Anticyclone to intensify its area and strength. The southern hemisphere storm tracks also shift poleward due to increased heating over the South Pacific Convergence Zone.

Key words: anticyclone; subtropical high pressure; SPCZ; South Pacific subtropical anticyclone; Rossby wave; tropical diabatic heating

1. Introduction

Subtropical Anticyclones (SAs) and the storm tracks are salient elements of the large-scale atmospheric circulation within both hemispheres. SAs are semi-permanent, high-pressure systems situated over each subtropical ocean basin that both influence and respond to Sea Surface Temperature (SST), precipitation, atmospheric moisture transport, and wind-driven ocean circulation. In the southern hemisphere, the South Pacific SA (SPSA), South Atlantic SA (SASA), and South Indian SA (SISA) dominate regional precipitation variability on sub-seasonal to decadal timescales over South America (Doyle and Barros 2002; Reboita et al. 2010), southern Africa (Burls et al. 2019), and Australia (Sturman and Tapper 1996).

SAs are primarily forced by upper-tropospheric radiative cooling and the associated descending motion within the Hadley cell that creates a high-pressure belt over the subtropical region in both hemispheres. However, the SAs themselves are locally more intense than the rest of the subtropical high-pressure belt. Bergeron (1930) was the first to make the distinction between the uniform subtropical high-pressure belt and the subtropical high-pressure systems over the subtropical oceans within the context of airmass and frontal development. The Hadley circulation is strongest in the winter hemisphere due to the enhanced meridional temperature gradient from the warm tropics to the cold winter hemisphere, and one might therefore expect the SAs to reach their seasonal maxima in local winter (Hoskins 1996; Lee et al. 2013). This expectation is however only true for the SASA and the SISA. The SAs in the NH reach their climatological maximum in both area and strength during local summer (Hoskins 1996; Rodwell and Hoskins 2001; Seager et al. 2003; Nigam and Chan 2009), as does the topic of this study the SPSA, raising the question, what else controls the area and strength of SAs?

Several studies have shown that the seasonal evolution in the strength of SAs is not only associated with the strength of Hadley cell descent but also local monsoonal heating over the surrounding continents. Hadley cell descent dominates the zonal mean component of SAs, whereas the surrounding subtropical landmass heating dominates the zonally asymmetric component. The importance of surrounding land monsoonal heating was first recognized by Ting (1994). Using a steady-state, linear, primitive equation model Ting (1994) analyzed the large-scale circulation due to local monsoonal heating, especially focusing on the Indian summer monsoon heating. Later, Hoskins (1996) argued that heating over the continents to the east of an ocean basin largely contributes to the summer intensification of its SA, which explains the North Pacific SAs maximum strength during local summer, June-July-August (JJA), when local Hadley cell descent is weak. The continental heating to the east of the ocean basin releases latent heat during the summer and generates a Rossby wave response to the northwest of the heated continent. The warm air from this monsoonal heating descends over the eastern flank of the adjacent ocean basin. Rodwell and Hoskins (2001) and Chen et al. (2001) later went on to demonstrate that heating on both continents surrounding an ocean basin contributes to the formation of SAs. Rodwell and Hoskins (2001) suggested that the equatorward portion of the SA forms as a Kelvin wave response to the monsoonal heating over the continent to the west of the ocean basin. For the SH, Rodwell and Hoskins (2001) argued that the orography of the SH continents plays a significant role in positioning SAs.

Wu and Liu (2003) and Liu et al. (2004) highlight that it is essentially diabatic heating differences between land and ocean that control the development of summer SAs. A quadrupole heating pattern of heating over the land and cooling over the eastern flank of subtropical oceans during local summer acts as a driver for the atmospheric circulation and the development of SAs (Wu and Liu 2003). In general, total diabatic heating differences act to cool the eastern flank of the ocean basins and warm the continents. The ocean regions are dominated by longwave cooling, the western flanks of the continents are dominated by sensible heating, and the eastern flanks of the continents are dominated by latent heating. This heating pattern gives rise to anticyclonic upper-troposphere circulation over the land, and cyclonic upper-troposphere circulation over the neighboring oceanic region, with cyclonic surface circulation over land and an anticyclonic surface circulation over the ocean. Wu and Liu (2003) proposed that this distinct circulation pattern exists as a response to the quadrupole heating. Seager et al. (2003) also

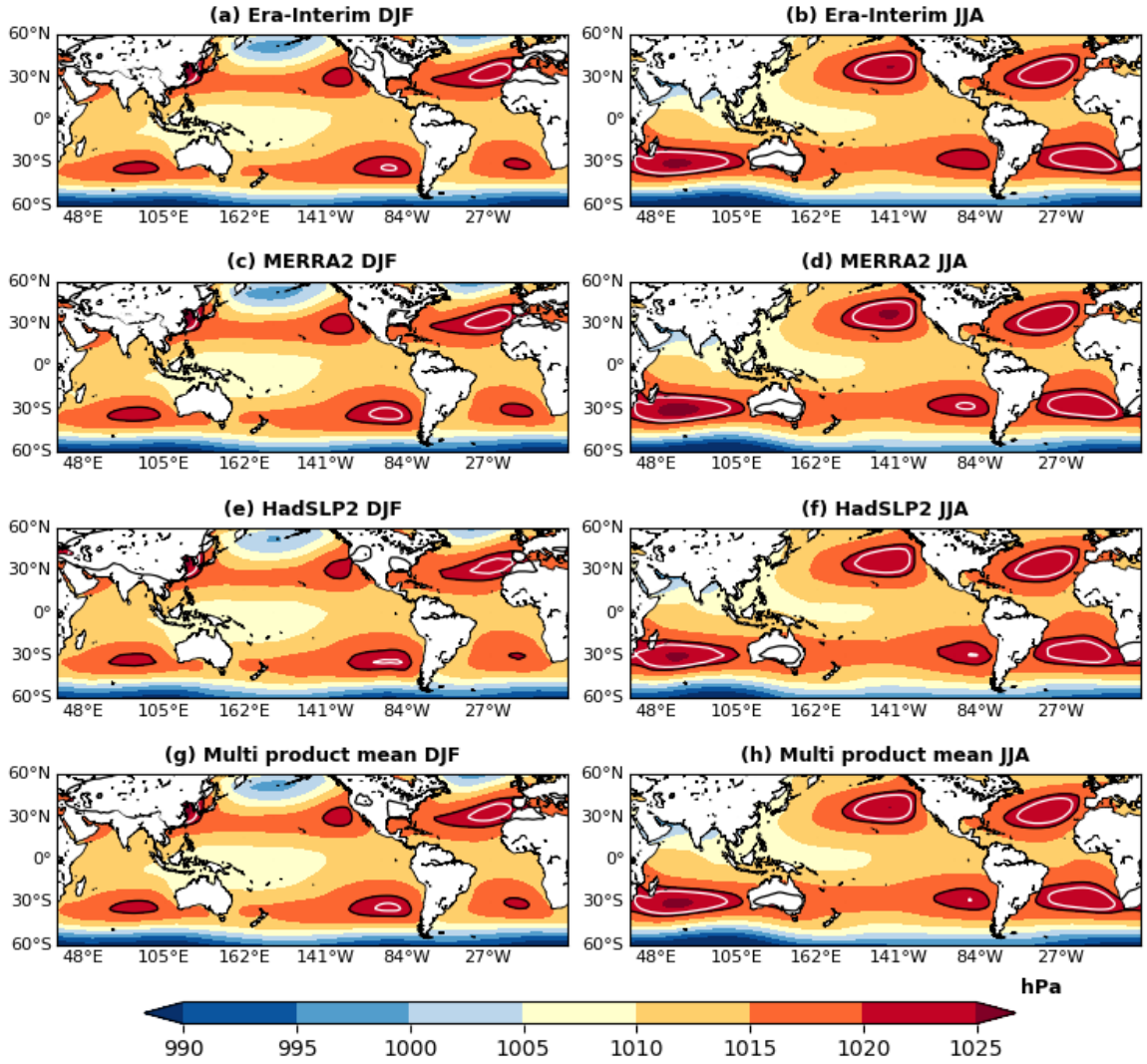

Fig. 1: SLP climatology (unit: hPa) for DJF (left panel) & JJA (right panel). The SLP climatology for both seasons is computed from (a-b) ERA-Interim (1979-2016), (c-d) MERRA2 (1980-2016), (e-f) HadSLP2 (1980-2016), & (g-h) the multi-product mean (average of ERA-Interim, MERRA2, & HadSLP2). The 1020hPa SLP is contoured in black and the 1022hPa SLP contoured in white.

argued that zonal asymmetries in SSTs can act as a secondary forcing in subtropical ocean basin and influence the seasonal strengthening of SAs.

The NH SAs reach their maximum strength during local summer (JJA) due to Asian, North African and North American summer monsoon heating contributing to the asymmetric component of the NH SAs despite the fact that the local Hadley cell descent is weak in this season (Hoskins 1996; Rodwell and Hoskins 2001; Nigam and Chan 2009; Chen et al. 2001). In the SH, local summer monsoonal heating is not as strong as that in the NH due to the smaller landmass-ocean ratio. As a result, the SH SASA and SISA reach their maximum during local (JJA) due to stronger Hadley cell descent during local winter, rather than local summer (Richter et al. 2008; Nigam and Chan 2009; Richter et al. 2010; Sun et al. 2017; Vizy and Cook 2016). Interestingly, this is not the case for the SPSA. As shown in Fig. 1, climatologically the SPSA is stronger during local summer, December-January-February (DJF), compared to the during JJA (local winter), whereas the seasonal cycle of the SASA and the SISA peak in area and strength during JJA (local winter). The SPSA's seasonal cycle in area and strength reaches its maximum during September-October-November, but remains intensified until February

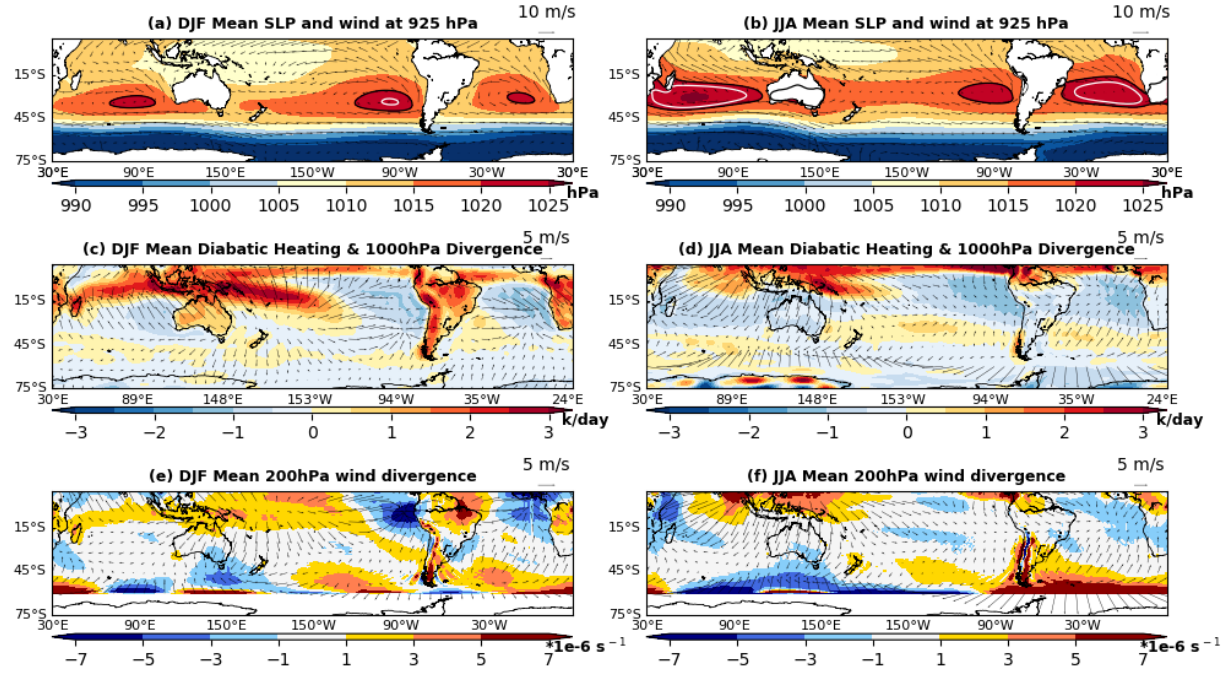

Fig. 2: Era-Interim (1979-2016) climatology of (a) DJF and (b) JJA mean of SLP (shaded) (unit: hPa), and 925hPa wind. The 1020hPa SLP is contoured in black and the 1022hPa SLP contoured in white. The 1022hPa contour is only present in the SPSA during DJF, and the SISA and SASA during JJA. Era-Interim (1979-2016) climatology of (c) DJF and (d) JJA vertical-mean diabatic heating (shaded) (unit: k/day), and the 1000hPa divergent wind component (vector). Era-Interim (1979-2016) climatology of (e) DJF and (f) JJA mean of 200hPa divergence (unit: s^{-1}). The wind component of divergence is plotted as vector (unit: m/s). The magnitude of divergence is scaled by 10^{-6}.

(Lee et al. 2013) (supplementary Fig. S1). This distinct climatological feature of the SPSA is consistently present in the ERA-Interim reanalysis dataset (Figs. 1a & 1b), the Modern-Era Retrospective analysis for Research and Applications, Version 2 (MERRA-2) (Figs. 1c & 1d), the Hadley Centre Sea Level Pressure (HadSLP2) (Figs. 1e & 1f), the Community Earth System Model (CESM) 2 (supplementary Fig. S2), and the multi-model-mean of Coupled Model Intercomparison Project (CMIP) phase 5 & 6 historical and future simulations (Fahad et al. 2020).

The deviation of zonal mean climatological SLP (climatological SLP – zonal mean climatological SLP) shows that the SPSA is the only SH SA that has a stronger asymmetric component during DJF than JJA (supplementary Fig. S3). In fact, the asymmetric SLP component of the SPSA is almost nonexistent in JJA (supplementary Fig. S3). Using the Community Atmospheric Model, Lee et al. (2013) show this phenomena exists in CAM. Without interhemispheric energy transfer the SPSA only exists as subtropical high pressure system during DJF, while the SISA and the SASA still reach a maximum in area and strength during JJA in the same experiment (other seasons not shown). Lee et al. (2013) also identify heating and cooling regions near the northern part of the tropics at 500hPa, and show how this tropical heating influences SAs in both hemispheres. Using a steady-state, linear primitive equation model that solves the sigma-coordinate equations linearized about a zonally symmetric basic state, Nigam and Chan (2009) show that adding heating over the tropical Pacific acts as a forcing on the North Pacific SA's seasonal development from winter to summer. They show that tropical heating over the Inter Tropical Convergence Zone (ITCZ) and South Pacific Convergence Zone (SPCZ) has a large influence on midlatitude atmospheric circulation and the seasonal evolution of the North Pacific SA. The influence of the SPCZ heating on the SH SAs

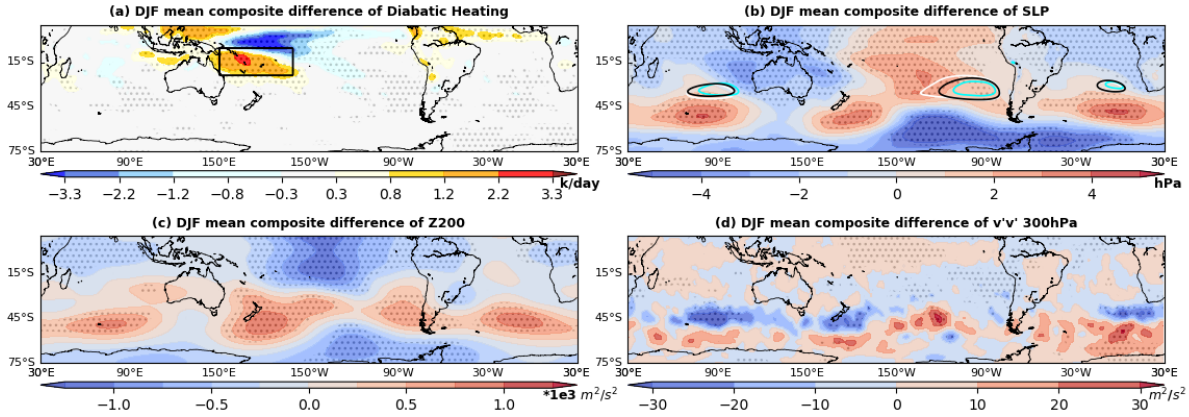

Fig. 3: The Era-Interim DJF mean composite difference between maximum heating years and minimum heating years over the SPCZ region (shown as black box) for (a) diabatic heating (unit: k/day), (b) SLP (unit: hPa), (c) Geopotential height at 200hPa (unit: m^2/s^2), and (d) v'v' at 300hPa (m^2/s^2). The 1020hPa SLP area of climatological SLP (1979-2016) (black), mean of maximum heating years (white), and mean of minimum heating years (blue) contoured in Fig.4b. The figures are stippled at 90% significance computed from t-test difference of mean on the sampled years.

climatological strength has however remained largely uninvestigated. The SPCZ is a unique feature over the southwestern Pacific Ocean with a spatial pattern of precipitation that is maximum during DJF (austral summer) and minimum in strength during JJA (austral winter). The vertically integrated diabatic heating associated with the SPCZ also has similar seasonality (Figs. 2c & 2d). The diabatic heating over the SPCZ region is maximum during DJF and shifts to its most southern position. The divergence of horizontal winds at 200hPa also shifts southward along with the SPCZ heating region.

The purpose of this paper is to use ERA-Interim Reanalysis and GCM experiments to determine the extent to which the heating over the SPCZ influences the large-scale circulation of the SH, specifically on the area and strength of the SPSA during DJF. Increased SPCZ heating changes the upper level divergence and divergent wind (advecting vorticity) which can act as a forcing to trigger a Rossby wave, significantly perturbing the balance of vorticity (James 1995; Holton and Hakim 2012). We hypothesize that the resultant Rossby wave train propagates into the extra-tropics, impacting surface pressure. The specific hypothesis to be tested is that during DJF, the changes forced by the SPCZ can directly project onto the SPSA, affecting its area and strength.

The study is structured as follows: description of methods and data used in this study are presented in Section 2; results of the study are broken down into Section 3 for the ERA-Interim reanalysis data and climate model analysis; and lastly Section 4 provides a summary and conclusions.

2. Methodology

The observationally-based data (years 1979-2016) used in this study is the ERA-Interim reanalysis product (Dee et al. 2011), MERRA2 (Gelaro et al. 2017), and HadSLP2 (Allan and Ansell 2006). Atmospheric diabatic heating is estimated from ERA-Interim data (following Swenson et al. 2019) and is computed from four times daily circulation and thermodynamic fields at the full horizontal resolution (512×256 Gaussian grid) and at 37 pressure levels, using a residual method similar to that of Hagos et al. (2010). The heating rate Q is obtained as:

$$Q = c_p \Pi \left(\frac{\partial \theta}{\partial t} + \vec{\nabla}.(\vec{v}\theta) - \theta\left(\vec{\nabla}.\vec{v}\right) + \omega\frac{\partial \theta}{\partial p}\right) \quad (1)$$

Where θ is potential temperature, p is pressure, c_p the specific heat at constant pressure, **v** the horizontal velocity, $\omega = \partial p/\partial t$, and $\Pi = (p/p_0)^{R/c_p}$ is the Exner function, where p_0 = 1000hPa and R is the gas constant. The heating was vertically integrated over the following nine layers (in units of hPa): 1000 – 925, 925 – 850,

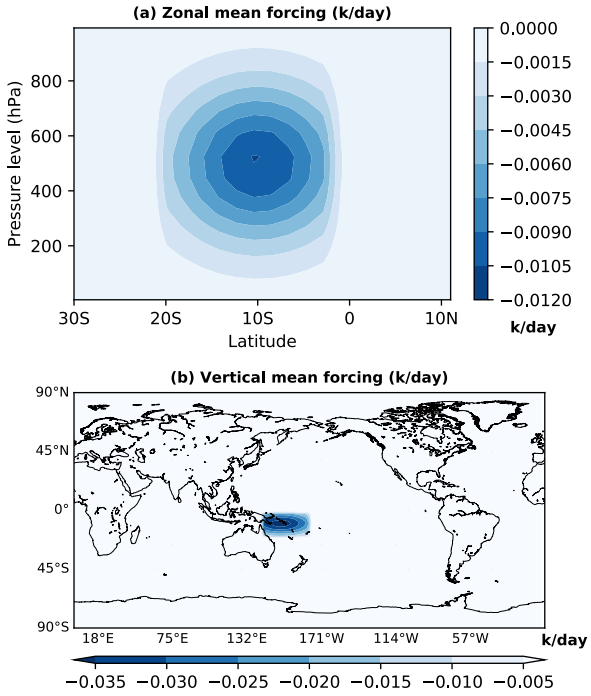

Fig. 4: (a) Zonal mean, and (b) vertical mean added heating structure of the Added Cooling experiments forcing file (units: k/day). Added Heating experiments has same added heating structure, except opposite sign.

850 – 775, 775 – 650, 650 – 550, 550 – 450, 450 – 350, 350 – 200 and 200 – 50. A composite analysis is performed in order to demonstrate how inter-annual variability in DJF SPCZ heating influences the SH large-scale circulation. For the composite analysis, the maximum (and minimum) heating years are selected based on vertically integrated DJF SPCZ heating during years that are greater (and lesser) than 1.2 standard deviations from the mean DJF SPCZ heating. The chosen domain of the SPCZ heating region is 150ºE-160ºW longitude and 24ºS-5ºS latitude. The maximum heating years in the composite are 1989, 1999, 2008, 2011, 2012 and minimum heating years are 1992, 1993, 1995, 2003, 2016. The ERA-Interim 1020hPa isobar area and position is used to identify the SH SAs.

Based on ERA-Interim composite analysis alone it is hard to isolate the SPCZ heating influence on SH large scale circulation and the SAs. While the compositing helps to isolate the role of SPCZ heating within inter-annual variability, diabatic heating changes outside of the SPCZ region are still evident (Fig. 3a). In particular there is evidence of an imprint from the El Niño Southern Oscillation (ENSO) (Figs. 3a and S4), which is not surprising given associations between SPCZ variability and ENSO.

To address this shortcoming and isolate the role of SPCZ heating, sets of AGCM experiments with variable SPCZ heating rates are carried out using the Community Atmosphere Model version 6 (CAM6), with prescribed climatological SST. CAM6 is the atmospheric component of the Community Earth System Model version 2 (Danabasoglu et al. 2020). The CAM6 numerical experiments are done with 1.9ºx2.5º resolution and the F2000climo component set forced with prescribed ERA-Interim reanalysis climatological SST (1979-2016).

The AGCM experiments with variable SPCZ heating consist of two sets of idealized experiments. The first set incorporates artificially weakened austral summer SPCZ heating (Added Cooling); the second set artificially intensified heating (Added Heating). These two sets each consist of 30 simulations and their DJF seasonal mean is compared to the DJF climatology from a 30-year-long control simulation. The control run is initialized using arbitrary atmospheric initial conditions, forced with monthly climatological SST and is run for 30 years. Subsequently, the seasonal runs are initialized November 1st as a branch run (from each November 1st of the control run) and run through to the following February with Added Cooling (Added Heating) applied to the SPCZ region. In these seasonal runs, a constant temperature tendency of ±0.12 K/day (15% of the total local climatological heating computed from the 30-year DJF climatology of the control run) is applied to the Added Cooling (and Added Heating) runs over the SPCZ region starting from November. Only DJF is considered for analysis (ignoring November, the first month of the add cooling/heating experiments). The cooling and heating were added (in addition to all other diabatic heating processes naturally generated by the model) along the DJF climatological position of the SPCZ with the maximum centered at 170ºE, 13ºS, and a vertical peak at the 500hPa level, with Gaussian decay away from the maximum heating (but still within the SPCZ region). The horizontal and vertical structure of the Added Heating is shown in the Fig. 4. The Added Cooling and Heating experiments are both forced with prescribed SST, identical to the control run.

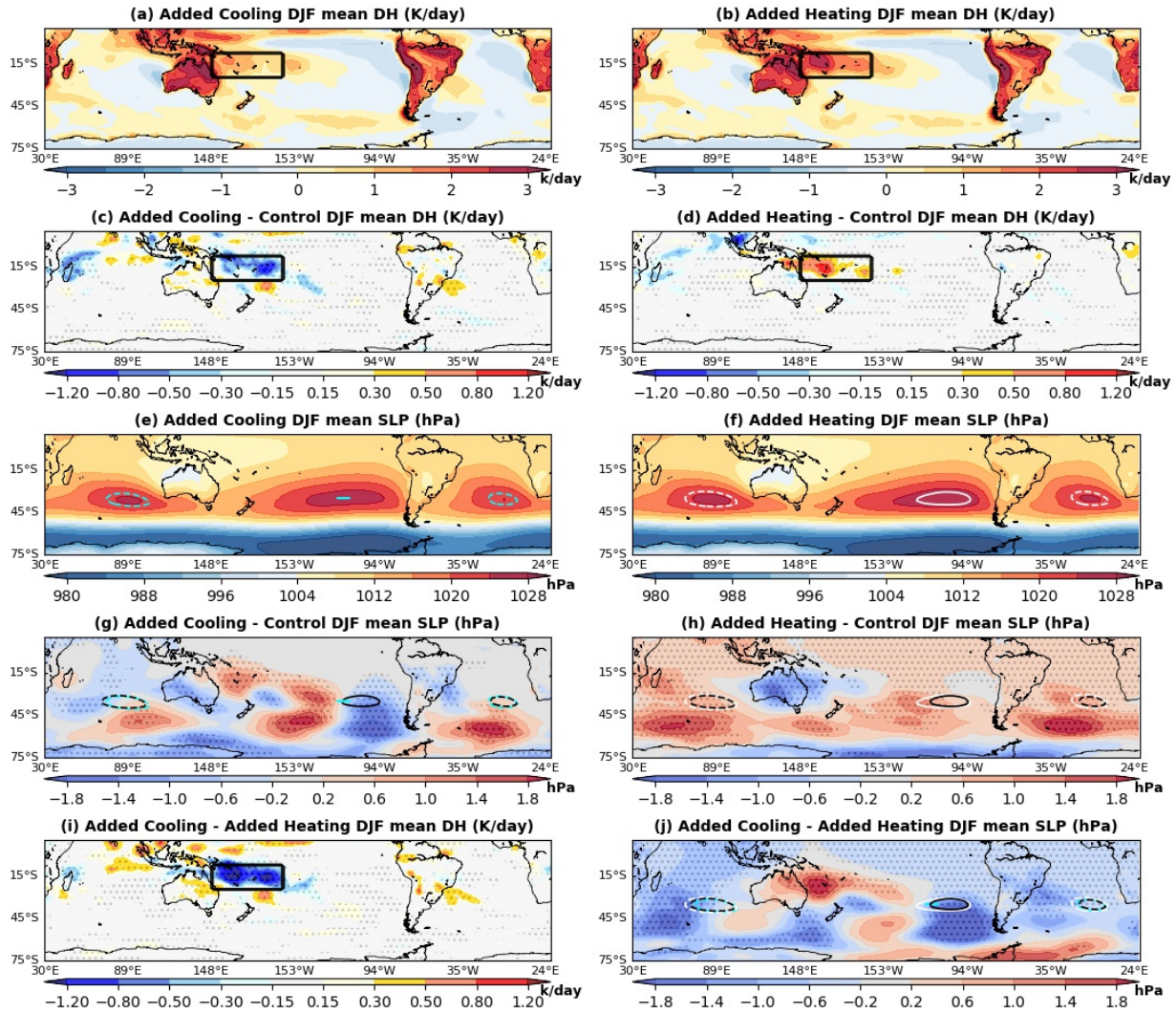

Fig. 5: 30-year DJF mean CESM2 CAM6 diabatic heating (unit: k/day) from (a) the Added Cooling runs, (b) the Added Heating runs, (c) the difference between the Added Cooling runs and the control run, and (d) the difference between the Added Heating runs and the Control run. The black box shows SPCZ heating region where the temperature tendency was added. Figs. 4e-h show the same analysis, except for SLP (unit: hPa). The center of each SA in the Control run is contoured in black, the Added Cooling runs in blue, and the Added Heating runs in white. A solid contour shows the 1025hPa isobar, and a dotted contour shows the 1022hPa isobar. The difference between the Added Cooling and Added Heating experiments is shown for (i) diabatic heating and (j) SLP. The figures are stippled at 95% significance computed using a difference of means t-test.

The CESM2 CAM6 30-year climatology shows similar SH seasonal characteristics to that in ERA-Interim. However, it largely overestimates the SLP over the subtropical regions compared to ERA-Interim reanalysis, especially over the SPSA. In order to analyze a similar area of the SAs, the 1022hPa isobar area is considered for the SASA and SISA, and the 1025hPa area is considered for the SPSA.

In order to study the influence of SPCZ heating on the storm track position, transient eddy momentum velocity variance U'U' and V'V' at 300hPa are analyzed. Here transients (U', V') are defined as all components of (U, V) with periods less than about 6 days, as obtained with a Butterworth filter. The strength of the upper-level storm track can be inferred from the transient eddy meridional velocity (V'V') at 300hPa.

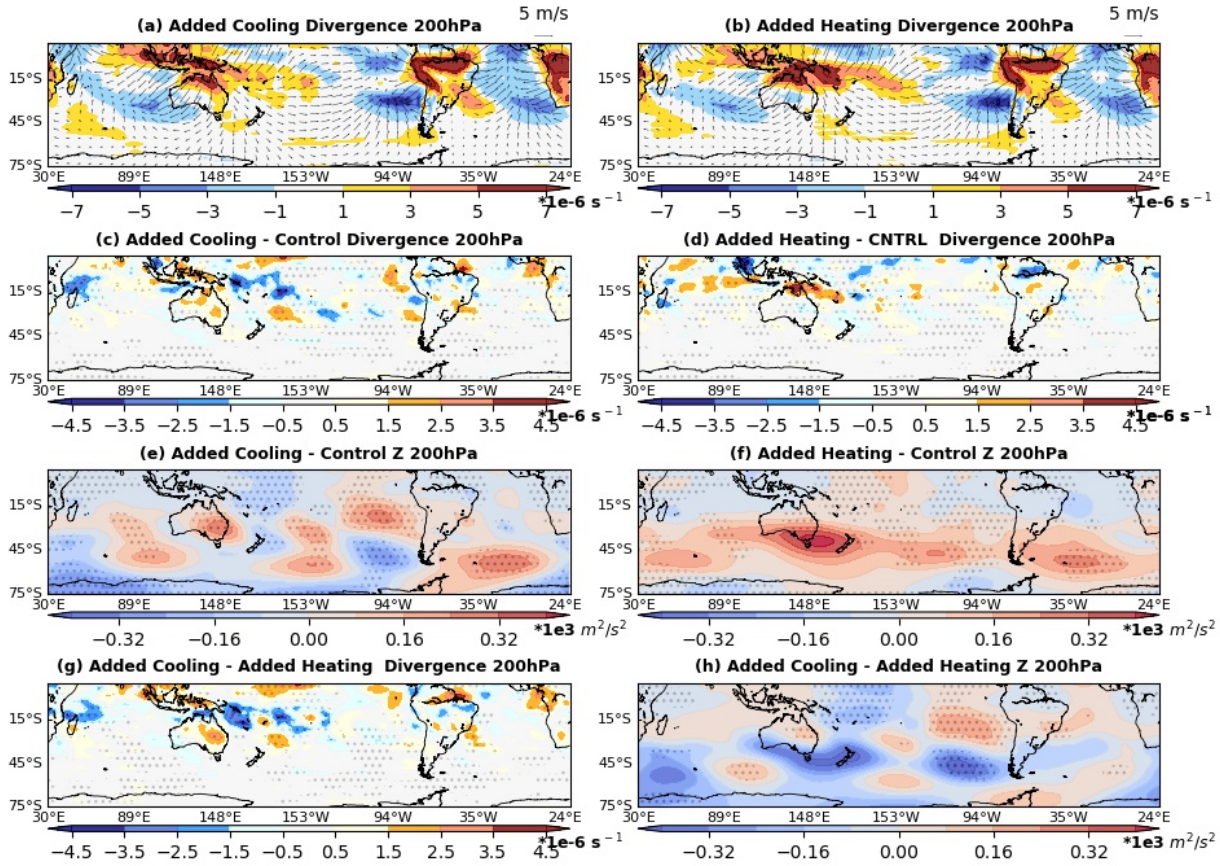

Fig. 6: 30-year DJF mean CESM2 CAM6 divergence at 200hPa (unit: *1e-6 s^{-1}) for (a) the Added Cooling runs, (b) the Added Heating runs, (c) the difference between the Added Cooling run and the controls run, and (d) the difference between the Added Heating runs and the control run. The 200hPa wind divergence is plotted as a vector (unit: m/s). The geopotential height at 200hPa (unit: *1e3 m^2s^{-2}) for (e) the difference between the Added Cooling runs and the control run, and (f) the difference between the Added Heating runs and the control run. The difference between the Added Cooling and Added Heating experiments is shown for (i) the divergence at 200hPa and (j) the geopotential height at 200hPa. The figures are stippled at 95% significance computed using a difference of means t-test.

3. Results

3.1. SPCZ Heating in the ERA-Interim Reanalysis

The DJF composite difference between maximum heating years and minimum heating years shows a shift in heating from the equatorward flank of the SPCZ to the climatological position of the SPCZ (Fig. 3a). The composite difference based on the same years shows a positive-negative SLP anomaly pattern over the SH subtropical and midlatitude region, consistent with the signature of a Rossby wave train (Fig. 3b). The wave train forced by the intensified SPCZ heating propagates poleward, appears to reach a turning latitude, and then propagate equatorward (as in Hoskins and Karoly, 1981). It is this equatorward-oriented branch which affects the SPSA. The wave train's positive SLP anomaly projects on to the SPSA leading to an increase in its strength and area. For the minimum heating years, the area enclosed by the 1020hPa contour (shown in blue) of the SPSA decreases compared to the climatological area (black contour) (Fig. 3b). In contrast, the 1020hPa area (white contour) increases and extends westward during maximum SPCZ heating years. Although positive/negative SLP anomalies associated with the Rossby wave train are present over the South Atlantic and South Indian Ocean basins, significant changes (as indicated by the stippling in Fig. 3b) are seen only over the poleward flank of the SASA and the SISA. Therefore, there are no significant changes in the area and strength of the centers of the SASA and the SISA. The geopotential height at 200hPa

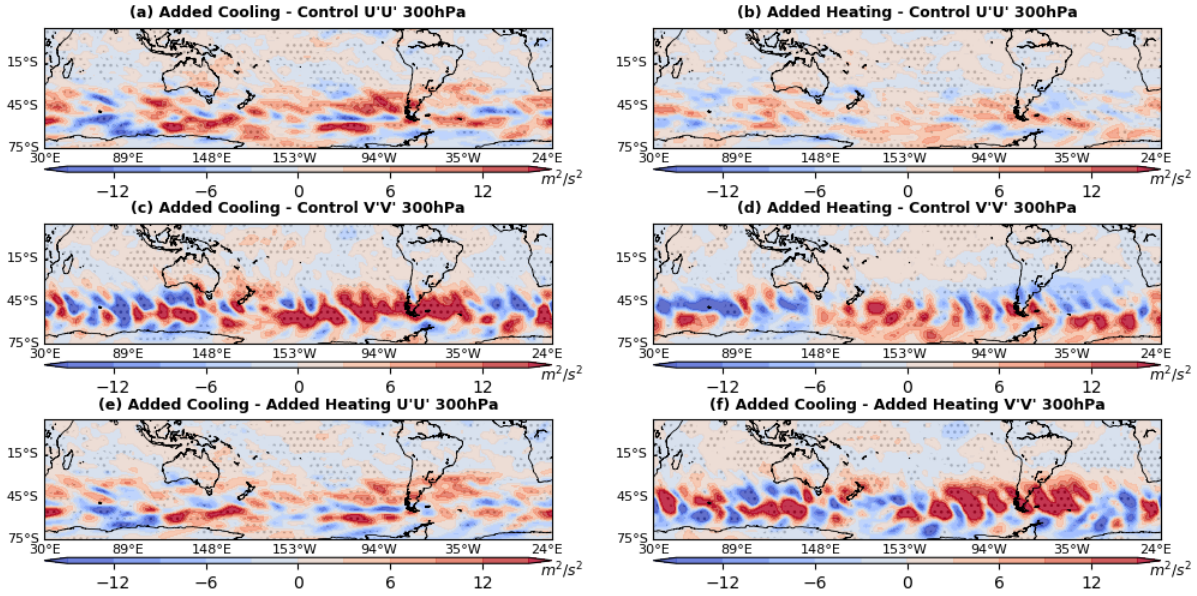

Fig. 7: 30-year DJF mean CESM2 CAM6 U'U' at 300hPa (unit: m^2s^2) for (a) the difference between the Added Cooling runs and the control run, (b) the difference between the Added Heating runs and the control run. V'V' at 300hPa (unit: m^2s^2) for (c) the difference between the Added Cooling runs and the control run, (d) the difference between the Added Heating runs and the control run. The difference between the Added Cooling runs and the Added Heating runs is shown for (e) U'U' at 300hPa and (f) V'V' at 300hPa.

(Z200) composite difference between maximum and minimum heating years shows qualitatively a similar response (Fig. 3c). A Z200 positive/negative height change similar to the Rossby wave train response is noticeable over the SH mid-latitude and subtropical regions. With increased heating over the SPCZ region, the Z200 height increases over the SPSAs center and poleward flank. There are however no significant Z200 height changes over the SASA and the SISA centers with the positive height changes in response to increases SPCZ heating confined to the poleward flanks of the SASA and the SISA.

The transient eddy variance (V'V') at 300hPa shows a physically-consistent response. The large belt of decreased SLP throughout the mid- to high-latitude SH shown in Fig. 3b is accompanied by a poleward shift in the storm tracks at most longitudes. However, the low pressure area extending towards the SASA in Fig. 3b (around 120°W and 50°S) is accompanied by an increase in eddy variance, somewhat to the south and west of the SASA.

As mentioned in the methods section, while this compositing approach helps to isolate the role of SPCZ heating within inter-annual SH SLP and storm track variability, it does not truly separate the role of the SPCZ from the influence of other modes of interannual variability. This motivates the analysis presented in the next section on the result from our prescribed SPCZ heating experiments.

3.2. CAM6 Numerical Heating Experiments

The DJF climatological mean SLP from the Added Cooling experiments shows significant changes in the SH subtropical and midlatitude atmospheric circulation compared to the control run (Fig. 5 a, c, e, & g). Due to a weakened SPCZ heating, a wave train of SLP anomaly pattern is generated over the SH subtropics (Fig. 5 e & g). The negative SLP anomaly pattern over the Pacific Ocean projects onto the center of the SPSA in response to weakened SPCZ heating, consistent with the change found in the ERA-Interim composite analysis. In the Added Cooling experiment, the area of the SPSA center (1025hPa contour) is very small. In contrast, in the Added Heating experiment, the size of the center of the SPSA increases and extends westward compared to the Control simulation (Fig. 5 f & h). Interestingly, SLP changes at the center of the SASA in the Added Cooling experiment (Fig. 5 g) is significant at the 95% level, but not in the Added Heating

experiment (Fig. 5h). In contrast, the Added Heating over the SPCZ region increases the SPSAs area and strength by generating Rossby wave SLP train anomalies (Fig. 5 b, d, f, & h). The extreme case scenario of Added Heating – Added Cooling experiments show the intensified SPSAs strength due to increased SPCZ heating during DJF (Fig. 5 i & j). We again see (in Figs. 5g and 5j) a strong suggestion of a poleward propagating wave train which reaches a turning latitude and then propagates equatorward, influencing the SASA.

Analysis of the 200hPa divergence in these simulation shows that a decrease in heating over the SPCZ region leads to a decrease in divergence and divergent wind (wind component of the divergence) in the upper troposphere (Figs. 6 a, c, &e). The SPCZ heating change triggers a Rossby wave train over the SH subtropics and midlatitudes by changing the upper-level divergence and divergent wind. The SLP anomalies and Z200 height changes due to changes in the heating are consistent, again showing a stationary Rossby wave which propagates poleward and turns. In the cooling experiment, there is a decrease in Z200 height consistent with the decrease in SLP over the center and poleward flank of the SPSA (Fig. 6e). In contrast, the Z200 height increases over the center of SPSA due to increased upper level divergence and heating over the SPCZ region (Figs. 6 b, d, &f). The Z200 response is consistent with the extreme SPCZ heating change scenario (Figs. 6 g & h).

The SPCZ heating also significantly influences the SH storm tracks strength and position. The transient eddy zonal velocity (U'U') at 300hPa and transient eddy meridional velocity (V'V') at 300hPa show that the strength of the SH storminess increases over the South Pacific Ocean near the SPSA due to a decrease of the SPCZ heating (Fig. 7 a & c). The storm track response seen in Fig. 7c is consistent with the wave train propagation seen in Fig. 6e, leading to increased storminess in a region just south of the SASA. The storm track response in the Added Heating experiment has a more ambiguous signature near the SASA (Figs. 7b and 7d). However, the Added Cooling minus Added Heating experiment storm track shifts (Figs. 7e and 7f) show the clear signature of the storm tracks influencing the SASA.

4. Conclusions and Discussion

The role of austral summer SPCZ heating on subtropical atmospheric circulation in the SH has been studied through a series of prescribed cooling/ heating experiments. During austral summer (DJF), the center of the SPSA is stronger compared to austral winter (JJA). This stands in contrast to the centers of the SASA and SISA, which reach their maximum in strength and area during austral winter (JJA). Previous studies have attributed the JJA maxima to enhanced NH monsoonal heating. The results of this study show that changes in the SPCZ heating, which reaches its seasonal maximum during DJF, leads to an enhancement of the area and strength of the center of the SPSA by generating a stationary Rossby wave that propagates poleward across the South Pacific into the SH midlatitudes, and then turns and propagates equatorward. It is noteworthy that the Added Cooling experiments show a much cleaner Rossby wave response (compared to the Control) than do the Added Heating experiments.

An SH midlatitude wave train of high- and low-pressure is consistent with an increased heating over the SPCZ region during DJF in ERA-Interim composite analysis. The positive SLP anomalies project onto the center of the SPSA, leading to an increase in area and strength. The Z200 height anomalies show a pattern of increased height consistent with an increased SLP anomaly.

The AGCM CAM6 is used to analyze the influence of the weakened and strengthened SPCZ heating on SH atmospheric circulation. Added Cooling and Added Heating prescribed SST experiments are compared with a Control run to investigate the influence of SPCZ heating during DJF. Results show there is a Rossby wave train of high and low pressure emanating poleward in the SH due to changes in upper-level divergence over the SPCZ in response to heating changes. The increased SPCZ heating anomalies force anomalous ascent leading to anomalous divergence aloft and hence perturbing the Rossby wave source term in the barotropic vorticity equation. The Rossby wave train response in the South Pacific Ocean basin occurs over the subtropical to mid-latitude regions, whereas in the South Atlantic and Indian Ocean regions the Rossby wave train response is only significant over the poleward flank of the SASA and the SISA. In contrast, weakened SPCZ heating leads to opposite Rossby wave train response over the SH subtropics and

midlatitudes that weakens the SPSAs area and strength. However, there is no significant SLP changes over the subtropics of South Indian and South Atlantic Ocean, except on the poleward flanks. The 200hPa geopotential height also shows a height increase over the SPSA in response to increased heating over the SPCZ region, and opposite response due to cooling over the SPCZ region.

The magnitude of SLP and Z200 changes in the SH associated with changes in the SPCZ heating are broadly consistent between the ERA-Interim composite analysis and the CAM6 heating experiments. This implies the imposed Added Heating change over the SPCZ region in the CAM6 numerical experiments are reasonable. In the CAM6 runs, there are some forced equatorial heating changes also visible (e.g. over the Maritime Continent) due to change of heating over the SPCZ region (Fig. 5 c & d). However, they are much smaller in size and magnitude compared to the SPCZ heating changes, and likely play a secondary role at best. There is also an opposite response of SLP and Z200 noticeable between CAM6 Added Heating runs and ERA-Interim (e.g. poleward of 45ºS at around 90ºW) (Fig. 3 & 5). This could be due to the influence of other modes of the interannual variability (e.g. Southern Annular Mode, local SST) in the ERA-Interim composite analysis.

The heating over the SPCZ region also significantly influences the strength and position of the SH storm tracks during austral summer (DJF). The transient heat and momentum fluxes and local diabatic heating associated with storm tracks act to indirectly amplify the forced response from tropical forcing (Held et al. 1989). So, it is important to understand how SH Storm tracks responses due to changes in the heating over the SPCZ. The SH storm track is shifted poleward due to the increased SPCZ heating in both ERA-Interim and CAM6. The baroclinic eddy growth and strength of storminess decreases where SLP associated with the Rossby wave train has positive anomalies due to change in the SPCZ heating. In contrast, weakened SPCZ heating leads to increased seasonal mean storminess over the equatorward SH storm tracks.

Although the seasonal cycles of SH SAs are similar, the area and strength of SAs are overestimated (~7-10hPa) in the CAM6 runs with prescribed SST compared to the ERA-Interim reanalysis (Fig. 1 & supplementary Fig. S2). A similar bias in the seasonal cycle of SA is also present in the coupled CESM model run from CMIP5 and CMIP6 simulation (Fahad et al. 2020). The bias in the SAs in the CAM6 during both seasons could be due to intensified local land-sea diabatic heating differences, overestimating tropical diabatic heating, or both. Future work will focus on the role of climatological biases in diabatic heating in the development of the climatological biases seen in the strength and seasonal cycle of the SH SAs and midlatitude atmospheric circulation in CAM6 prescribed SST and coupled CESM historical simulations.

Acknowledgements

This study was supported by the National Science Foundation (NSF; AGS-1613318, AGS-1338427), the National Aeronautics and Space Administration (NASA; NNX14AM19G), and the National Oceanic and Atmospheric Administration (NOAA; NA14OAR4310160). N.J.B. is supported by the Alfred P. Sloan Foundation as a Research Fellow. We acknowledge high-performance computing and analysis support from Cheyenne (https://doi.org/10.5065/D6RX99HX) provided by NCAR's Computational and Information Systems Laboratory, sponsored by the NSF. We also acknowledge ECMWF for use of the Era-Interim reanalysis dataset downloaded from https://www.ecmwf.int/en/forecasts/datasets/reanalysis-datasets/era-interim.

References

Allan, R., and T. Ansell, 2006: A new globally complete monthly historical gridded mean sea level pressure dataset (HadSLP2): 1850-2004. *J. Clim.*, doi:10.1175/JCLI3937.1.

Bergeron, T., 1930: Richlinien einer dynamischen klimatologie. *Meteorol. Zeitschrift*, **47**, 246–262.

Burls, N. J., R. C. Blamey, B. A. Cash, E. T. Swenson, A. al Fahad, M.-J. M. Bopape, D. M. Straus, and C. J. C. Reason, 2019: The Cape Town "Day Zero" drought and Hadley cell expansion. *npj Clim. Atmos. Sci.*, **2**, 27, doi:10.1038/s41612-019-0084-6. https://doi.org/10.1038/s41612-019-0084-6.

Chen, P., M. P. Hoerling, and R. M. Dole, 2001: The origin of subtropical anticyclones. *J. Atmos. Sci.*, **58**, 1827–1835, doi:10.1175/1520-0469(2001)058<1827:TOOTSA>2.0.CO;2.

Danabasoglu, G., and Coauthors, 2020: The Community Earth System Model Version 2 (CESM2). *J. Adv. Model. Earth Syst.*, **12**, doi:10.1029/2019MS001916. https://onlinelibrary.wiley.com/doi/abs/10.1029/2019MS001916.

Dee, D. P., and Coauthors, 2011: The ERA-Interim reanalysis: Configuration and performance of the data assimilation system. *Q. J. R. Meteorol. Soc.*, **137**, 553–597, doi:10.1002/qj.828.

Doyle, M. E., and V. R. Barros, 2002: Midsummer low-level circulation and precipitation in subtropical South America and related sea surface temperature anomalies in the South Atlantic. *J. Clim.*, **15**, 3394–3410.

Fahad, A. al, N. J. Burls, and Z. Strasberg, 2020: How will southern hemisphere subtropical anticyclones respond to global warming? Mechanisms and seasonality in CMIP5 and CMIP6 model projections. *Clim. Dyn.*, doi:10.1007/s00382-020-05290-7. http://link.springer.com/10.1007/s00382-020-05290-7.

Gelaro, R., and Coauthors, 2017: The modern-era retrospective analysis for research and applications, version 2 (MERRA-2). *J. Clim.*, **30**, doi:10.1175/JCLI-D-16-0758.1.

Held, I. M., S. W. Lyons, and S. Nigam, 1989: Transients and the Extratropical Response to El Niño. *J. Atmos. Sci.*, **46**, 163–174, doi:10.1175/1520-0469(1989)046<0163:TATERT>2.0.CO;2. http://journals.ametsoc.org/doi/abs/10.1175/1520-0469%281989%29046%3C0163%3ATATERT%3E2.0.CO%3B2.

Hoskins, B., 1996: On the Existence and Strength of the Summer Subtropical Anticyclones. *Bull. Am. Meteorol. Soc.*, **77**, 1287–1292.

Hoskins, B. J., and D. J. Karoly, 1981: The Steady Linear Response of a Spherical Atmosphere to Thermal and Orographic Forcing. *J. Atmos. Sci.*, **38**, 1179–1196, doi:10.1175/1520-0469(1981)038<1179:TSLROA>2.0.CO;2. http://journals.ametsoc.org/doi/abs/10.1175/1520-0469%281981%29038%3C1179%3ATSLROA%3E2.0.CO%3B2.

Lee, S. K., C. R. Mechoso, C. Wang, and J. D. Neelin, 2013: Interhemispheric influence of the northern summer monsoons on southern subtropical anticyclones. *J. Clim.*, **26**, 10193–10204, doi:10.1175/JCLI-D-13-00106.1.

Liu, Y., G. Wu, and R. Ren, 2004: Relationship between the subtropical anticyclone and diabatic heating. *J. Clim.*, **17**, 682–698, doi:10.1175/1520-0442(2004)017<0682:RBTSAA>2.0.CO;2.

Nigam, S., and S. C. Chan, 2009: On the summertime strengthening of the Northern Hemisphere Pacific sea level pressure anticyclone. *J. Clim.*, **22**, 1174–1192,

doi:10.1175/2008JCLI2322.1.

Reboita, M. S., M. A. Gan, R. P. da Rocha, and T. Ambrizzi, 2010: Precipitation regimes in South America: a bibliography review. *Rev. Bras. Meteorol.*, **25**, 185–204.

Richter, I., C. R. Mechoso, and A. W. Robertson, 2008: What determines the position and intensity of the South Atlantic anticyclone in austral winter? - An AGCM study. *J. Clim.*, **21**, 214–229, doi:10.1175/2007JCLI1802.1.

——, S. K. Behera, Y. Masumoto, B. Taguchi, N. Komori, and T. Yamagata, 2010: On the triggering of Benguela Niños: Remote equatorial versus local influences. *Geophys. Res. Lett.*, **37**, doi:10.1029/2010GL044461.

Rodwell, M. J., and B. J. Hoskins, 2001: Subtropical anticyclones and summer monsoons. *J. Clim.*, **14**, 3192–3211, doi:10.1175/1520-0442(2001)014<3192:SAASM>2.0.CO;2.

Seager, R., R. Murtugudde, N. Naik, A. Clement, N. Gordon, and J. Miller, 2003: Air-sea interaction and the seasonal cycle of the subtropical anticyclones. *J. Clim.*, **16**, 1948–1966, doi:10.1175/1520-0442(2003)016<1948:AIATSC>2.0.CO;2.

Sturman, A. P., and N. J. Tapper, 1996: *The weather and climate of Australia and New Zealand*.

Sun, X., K. H. Cook, and E. K. Vizy, 2017: The South Atlantic subtropical high: Climatology and interannual variability. *J. Clim.*, **30**, 3279–3296, doi:10.1175/JCLI-D-16-0705.1.

Swenson, E. T., D. M. Straus, C. E. Snide, and A. Al Fahad, 2019: The Role of Tropical Heating and Internal Variability in the California Response to the 2015/16 ENSO Event. *J. Atmos. Sci.*, **76**, 3115–3128, doi:10.1175/JAS-D-19-0064.1. http://journals.ametsoc.org/doi/10.1175/JAS-D-19-0064.1.

Ting, M., 1994: Maintenance of Northern Summer Stationary Waves in a GCM. *J. Atmos. Sci.*, **51**, 3286–3308, doi:10.1175/1520-0469(1994)051<3286:monssw>2.0.co;2.

Vizy, E. K., and K. H. Cook, 2016: Understanding long-term (1982–2013) multi-decadal change in the equatorial and subtropical South Atlantic climate. *Clim. Dyn.*, **46**, 2087–2113, doi:10.1007/s00382-015-2691-1.

Wu, G., and Y. Liu, 2003: Summertime quadruplet heating pattern in the subtropics and the associated atmospheric circulation. *Geophys. Res. Lett.*, **30**, n/a-n/a, doi:10.1029/2002GL016209. http://doi.wiley.com/10.1029/2002GL016209.